Proton radii of Be, B, and C isotopes

Yoshiko Kanada-En'yo
Department of Physics, Kyoto University, Kyoto 606-8502, Japan

We investigate the neutron number (N) dependence of root mean square radii of point proton distribution (proton radii) of Be, B, and C isotopes with the theoretical method of variation after spin-parity projection in the framework of antisymmetrized molecular dynamics (AMD). The proton radii in Be and B isotopes changes rapidly as N increases, reflecting the cluster structure change along the isotope chains, whereas, those in C isotopes show a weak N dependence because of the stable proton structure in nuclei with $Z = 6$. In neutron-rich Be and B isotopes, the proton radii are remarkably increased by the enhancement of the two-center cluster structure in the prolately deformed neutron structure. We compare the N dependence of the calculated proton radii with the experimental ones reduced from the charge radii determined by isotope shift and those deduced from the charge changing interaction cross section. It is found that the N dependence of proton radii can be a probe to clarify enhancement and weakening of cluster structures.

arXiv:1411.0765v1 [nucl-th] 4 Nov 2014

I. INTRODUCTION

In light unstable nuclei, various exotic structures such as the magic number breaking, new cluster structures, and the neutron halo structure, have been discovered. In a series of Be isotopes, it has been revealed that the structure changes rapidly with the increase of the neutron number N and the cluster structure develops in neutron-rich Be isotopes as discussed in many theoretical and experimental studies [1–26]. The cluster structure in the ground states of ^{11}Be and ^{12}Be is considered to play an important role in the vanishing of the neutron magic number $N = 8$. For ^{11}Be, the breaking of $N = 8$ shell has been known experimentally from the abnormal spin-parity $1/2^+$, and for ^{12}Be, it has been suggested by slow β decay [27] and more directly evidenced by the intruder configuration observed in $1n$-knockout reactions [28, 29] as well as other experiments [30–32]. These nuclei have the largely deformed ground states with intruder neutron configurations having more remarkable cluster structure than the neighboring isotope, ^{10}Be.

Also in neutron-rich B isotopes, the enhancement of cluster structures has been theoretically predicted [33], whereas, in neutron-rich C isotopes, no cluster structure is predicted to develop at least in the ground states [2, 34, 35]. These facts indicate that the development of cluster structure strongly depends on proton and neutron numbers of the system. A problem to be solved is how one can experimentally observe the structure change along the isotope chain, i.e., the enhancement and weakening of the cluster structure with the increase of the neutron number N. Since the enhanced cluster structure in neutron-rich nuclei enlarges the deformation and spatial extent of proton density, the change of the cluster structure may affect such observables as electric quadrupole moments and charge radii. The former is not necessarily a direct information of proton structure because it is sensitive not only to the proton distribution but also to the neutron configuration through the angular momentum coupling. Moreover, it gives no information for the $J^\pi = 0^+$ ground states of even-even nuclei, in which the quadrupole moment is trivially zero. The latter, the charge radius, is usually not sensitive to the neutron configuration and it reflects more directly the proton density, at least for the radial extent, and therefore, the N dependence of the charge radius can be a probe to clarify the change of the cluster structure.

Recently, root mean square (rms) charge radii of neutron-rich Be isotopes have been precisely measured by means of isotope shift. In the systematics of charge radii in Be isotopes, the large charge radii of ^{11}Be and ^{12}Be, which have been recently measured, can be understood by the remarkable cluster structure in the deformed ground states of ^{11}Be and ^{12}Be [36, 37]. For neutron-rich B and C isotopes, change radii have yet to be measured except for ^{14}C near the stability line. Instead of isotope shift measurement, recently, a new experimental approach to determine rms radii of point-proton density (proton radii) by the charge changing interaction cross section has been proposed and applied to B and C isotopes [38, 39].

Our aim here is to clarify how the structure change with the N increase is reflected in proton radii. For this aim, we investigate the N dependence of proton radii in the isotope chains of Be, B, and C and the influence of change of cluster structures and intrinsic deformations on proton radii. We try to answer the question whether the N dependence proton radii can be a probe for the cluster structure in neutron-rich nuclei.

In this study, we calculate the ground states of Be, B, and C isotopes with the method of antisymmetrized molecular dynamics (AMD) [2]. The method has been proven to be a useful approach to describe structures, in particular, cluster structures, in light neutron-rich nuclei. Systematic studies with the simple version of AMD have predicted that structures of Be and B isotopes change rapidly with the increase of the neutron number [2, 7, 33]. Advanced studies with the variation after spin and parity projections (VAP) in the AMD framework have described the breaking

of $N = 8$ magicity in neutron-rich Be [15, 16]. The latter method (the AMD+VAP) describes better the details of structures in ground and excited states than the former method (the simple AMD), in which the variation is performed before the spin projection. In the present study, we apply the AMD+VAP to Be, B, and C isotopes, and discuss the structure change focusing on the N dependence of the proton radius in each series of isotopes.

The paper is organized as follows. We describe the framework of the AMD+VAP in Section II, and show the results of Be, B, and C isotopes in Section III. Section IV discusses the structure change with the N increase and its influence on proton radii. The paper concludes with a summary in Section V.

II. FORMULATION OF AMD+VAP

We describe Be, B, and C isotopes with AMD wave functions by applying the VAP method. For the detailed formulation of the AMD+VAP, please refer to Refs. [10, 15, 16]. The method is basically the same as that used in those previous studies. A difference in the present calculation from Refs. [10, 15, 16] is that we do not adopt an artificial barrier potential, which has been used in previous studies to describe highly excited resonance states.

A. AMD wave functions

An AMD wave function is given by a Slater determinant of Gaussian wave packets;

$$\Phi_{\rm AMD}(\mathbf{Z}) = \frac{1}{\sqrt{A!}}\mathcal{A}\{\varphi_1, \varphi_2, ..., \varphi_A\}, \tag{1}$$

where $\mathcal{A}$ is the antisymmetrizer, and the ith single-particle wave function is written by a product of spatial(ϕ_i), intrinsic spin(χ_i) and isospin(τ_i) wave functions as,

$$\varphi_i = \phi_{\mathbf{X}_i}\chi_i\tau_i, \tag{2}$$

$$\phi_{\mathbf{X}_i}(\mathbf{r}_j) = \left(\frac{2\nu}{\pi}\right)^{4/3} \exp\{-\nu(\mathbf{r}_j - \frac{\mathbf{X}_i}{\sqrt{\nu}})^2\}, \tag{3}$$

$$\chi_i = (\frac{1}{2} + \xi_i)\chi_\uparrow + (\frac{1}{2} - \xi_i)\chi_\downarrow. \tag{4}$$

$\phi_{\mathbf{X}_i}$ and χ_i are spatial and spin functions, and τ_i is the isospin function fixed to be up (proton) or down (neutron). Accordingly, an AMD wave function is expressed by a set of variational parameters, $\mathbf{Z} \equiv \{\mathbf{X}_1, \mathbf{X}_2, \ldots, \mathbf{X}_A, \xi_1, \xi_2, \ldots, \xi_A\}$, indicating single-nucleon Gaussian centroids and spin orientations for all nucleons.

These parameters are determined by the energy variation after spin-parity projection to obtain optimized AMD wave functions for J^π states. Namely, in the AMD+VAP method, the parameters $\mathbf{X}_i$ and $\xi_i (i = 1 \sim A)$ for the lowest J^π state are determined so as to minimize the energy expectation value of the Hamiltonian, $\langle\Phi|H|\Phi\rangle/\langle\Phi|\Phi\rangle$, with respect to the spin-parity eigen wave function projected from an AMD wave function; $\Phi = P^{J^\pi}_{MK}\Phi_{\rm AMD}(\mathbf{Z})$. Here, $P^{J^\pi}_{MK}$ is the spin-parity projection operator.

In the present calculation, we choose the width parameter ν for single-nucleon Gaussian wave packets to minimize energies of stable nuclei (^{9}Be, ^{11}B, and ^{12}C) and use the fixed ν value in each series of isotopes. The adopted ν values are $\nu = 0.20$ fm^{-2} for Be isotopes, and $\nu = 0.19$ fm^{-2} for B and C isotopes. The fixing ν parameter may not be appropriate to describe details of neutron distribution in very neutron-rich nuclei. However, since our main concern in the present study is systematics of proton distribution, we fix the parameter to remove a possible artifact in proton radii caused by the change of ν. If the size of cluster cores in neutron-rich nuclei does not change from that in stable nuclei, the fixing ν can be a reasonable assumption. For more detailed study, different width parameters for protons and neutrons or independent widths for all nucleons should be adopted as done in the method of fermionic molecular dynamics (FMD) [40, 41] and an extended version of AMD [42].

In the AMD framework, the existence of clusters is not assumed *a priori*, but Gaussian centroids of all single-nucleon wave packets are independently treated. Nevertheless, if the system favors a specific cluster structure such the structure is automatically obtained by the energy variation because the AMD model space contains wave functions for various cluster structures.

We comment here that, in the simple AMD used in Refs. [7, 33], the energy variation was performed not after but before the spin projection (the variation before projection:VBP) for the AMD wave function with fixed single-nucleon intrinsic spins. In the present study, an advanced method, the AMD+VAP, in which the VAP is performed for the AMD wave function with flexible intrinsic spins, is adopted. The AMD+VAP method better describes structures of

the ground and excited states of light nuclei and also useful to investigate details of the structure change between shell-model-like states and cluster states than the simple AMD.

Note that the AMD wave function is similar to the wave function used in FMD calculations [41], though some differences exist in the width parameter and variational procedure, as well as adopted effective interaction.

III. RESULTS

A. effective interactions

In the present calculation of Be and B isotopes, we used the same effective nuclear interaction as that used for ^{11}Be and ^{12}Be in previous studies [15, 16]. It is the MV1 force [43] for the central force supplemented by a two-body spin-orbit force with the two-range Gaussian form same as that in the G3RS force [44]. The Coulomb force is approximated using a seven-range Gaussian form. Namely, we use the interaction parameters, $m = 0.65$, $b = 0$, and $h = 0$, for the Majorana, Bartlett, and Heisenberg terms of the central force, and the strengths $u_I = -u_{II} = 3700$ MeV of the spin-orbit force in the calculation of Be and B isotopes. The breaking of the $N = 8$ magicity in ^{11}Be and ^{12}Be is successfully described with this set of interaction parameters as discussed in the previous studies [15, 16]. For C isotopes, we use $m = 0.62$ and $b = h = 0$ for the central force, which is the parametrization same as that used for ^{12}C in the previous AMD+VAP calculation [45, 46]. In the present calculation of C isotopes, we tune the spin-orbit force strength and use $u_I = -u_{II} = 2600$ MeV so as to reproduce the experimental excitation energies of the 2^+_1 states in C isotopes.

B. Experimental data of rms proton and matter radii

In the comparison of the calculated proton radii with the experimental data, we reduce the rms proton radii (r_p) from the rms charge radii (r_c) determined by isotope shift measurements as,

$$r_p = \sqrt{r_c^2 - R_p^2}, \tag{5}$$

where $R_p = 0.8$ fm is the rms charge radii of an isolate proton. The experimental data of the charge radii for Be isotopes, ^{11}B, and ^{12,14}C are taken from Refs. [36, 37, 47].

In the experimental studies of the charge changing interaction cross section ($\sigma_{\rm cc}$), the proton radii have been deduced from a Glauber model analysis of the $\sigma_{\rm cc}$. We label thus deduced proton radii as $r_{\rm cc;G}$ in the present paper. The $r_{\rm cc;G}$ of neutron-rich B isotopes have been deduced from the $\sigma_{\rm cc}$ at $\sim$900 MeV/u in Ref. [39], and those of neutron-rich C isotopes have been deduced from the $\sigma_{\rm cc}$ at $\sim$300 MeV/u in Ref.[38].

We also perform a rough evaluation of the proton radii of B and C isotopes from the experimental data of the $\sigma_{\rm cc}$ at $\sim$900 MeV/u on the C target in Ref. [48] using a following simple ansatz,

$$\sigma_{\rm cc} = F\pi(r_p + r_{m,^{12}{\rm C}})^2, \tag{6}$$

where $r_{m,^{12}{\rm C}}$ is the rms matter radius of the target nucleus, ^{12}C, and F is the normalization factor for this beam energy. We assume $r_{m,^{12}{\rm C}}$ equals to the proton radius r_p of ^{12}C, which is experimentally known from the charge radius, and determine the factor F by the $\sigma_{\rm cc}$ for ^{12}C beam in the same experiment.. Using the common factor F determined by the inputs of r_p and $\sigma_{\rm cc}$ for ^{12}C, we evaluate the proton radii for B and C isotopes from the $\sigma_{\rm cc}$ in Ref. [48]. We call thus evaluated proton radii with the simple ansatz of Eq. 6 as $r_{\rm cc:S}$. Since there are many available data of the $\sigma_{\rm cc}$ for various neutron-rich isotopes in Ref. [48], this evaluation is helpful to see the N dependence of proton radii up to $N = 14$ in B and C isotopes.

As for the rms matter radii, the radii $r_{\rm I}$ were deduced from the interaction cross section $\sigma_{\rm I}$ using the Glauber analysis [49]. Consistency of the matter radii determined by the Glauber analysis at various beam energies has been checked (see Ref. [49] and references therein).

C. Be and B isotopes

We perform the AMD+VAP calculation for the ground states of Be and B isotopes. For ^{12}Be, in which two 0^+ states degenerate in the low-energy region, we also calculate the 0^+_2 state by the VAP with respect to the orthogonal

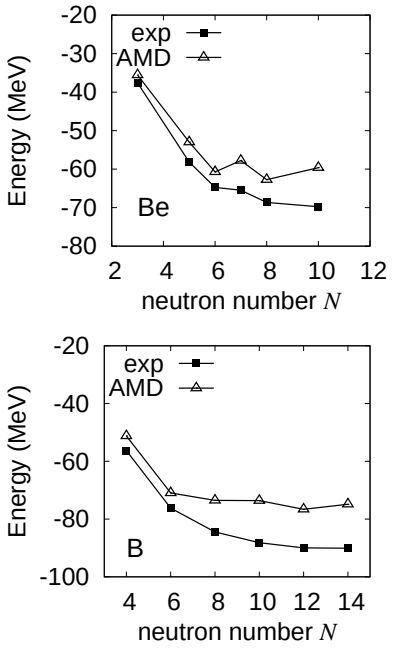


FIG. 1: Binding energy of Be and B isotopes. The theoretical values are calculated with the AMD+VAP using MV1($m = 0.65$)+LS($u_I = -u_{II} = 3700$ MeV) force. $\nu = 0.20$ fm^{-2} and 0.19 fm $^{-2}$ are used for Be and B isotopes, respectively. .

component to the 0_1^+ state, and superpose the obtained two AMD wave functions for the 0_1^+ and 0_2^+ states to take into account mixing of the configurations.

Figure 1 shows the binding energy of Be and B isotopes. The reproduction of the experimental biding energy in the present calculation is not perfect because of the limitation of the effective interaction. The reproduction can be improved by fine tuning of the interaction parameters or by introducing mass dependent interaction parameters. However, in the present study, we use the same parameters as the previous studies, which can describe the breaking of neutron magicity, to discuss the structure change long the isotopes, focusing on structure of protons.

Figure 2 shows the rms radii of proton, neutron, and matter distributions of Be isotopes. For ^{12}Be, we show radii calculated after and before the superposition of two AMD wave functions for $0_{1,2}^+$ obtained by the VAP. The proton radius is relatively large in ^{7}Be and also in ^{9}Be because of the remarkable cluster structure. As the neutron number N increases, the proton radius becomes the smallest in ^{10}Be at $N = 6$ and it increases in ^{11}Be and ^{12}Be, which have dominantly the intruder neutron configuration, and becomes larger in ^{14}Be. The increase of the proton radii in the $N \geq 6$ region reflects the development of cluster structure.

The N dependence of the proton radius is consistent with the experimental data reduced from the charge radii determined by isotope shift measurements. The trend of the N dependence of the present result is also similar to the FMD predictions in the $N \leq 8$ region [37]. For ^{14}Be, the present calculation predicts an increase of the proton radius because of the further development of the cluster structure and deformation, whereas the FMD calculation does not show such an increase in ^{14}Be.

In the present result, the neutron radius grows more rapidly in the $N \geq 6$ region as N increases than the proton radius. The N dependence of the matter radius, which is mainly determined by that of the neutron radius, is consistent with the experimental matter radii $r_{\rm I}$ deduced from the interaction cross section [49] except for a jump at $N = 7$ in the experimental data. The extremely large matter radius in ^{11}Be is caused by the neutron-halo structure, which is not described well in the present calculation because the wave function is limited to a Gaussian form and is not enough to describe the long tail of the halo neutron in the framework of the AMD+VAP.

Figure 3 shows the rms radii for B isotopes. As N increases, the calculated proton radius becomes smallest at $N = 6$ and increases in the $6 \leq N \leq 12$ region in consequence of the developed cluster structure in the deformed neutron structure. The proton radius decreases from $N = 12$ to $N = 14$ because of the weakening of the cluster structure in ^{19}B. Note that the weakening of the cluster structure in ^{19}B has not been obtained in the previous study in Ref. [33], in which the adopted spin-orbit force was too weak to describe the shape coexistence in $N = 14$ isotones

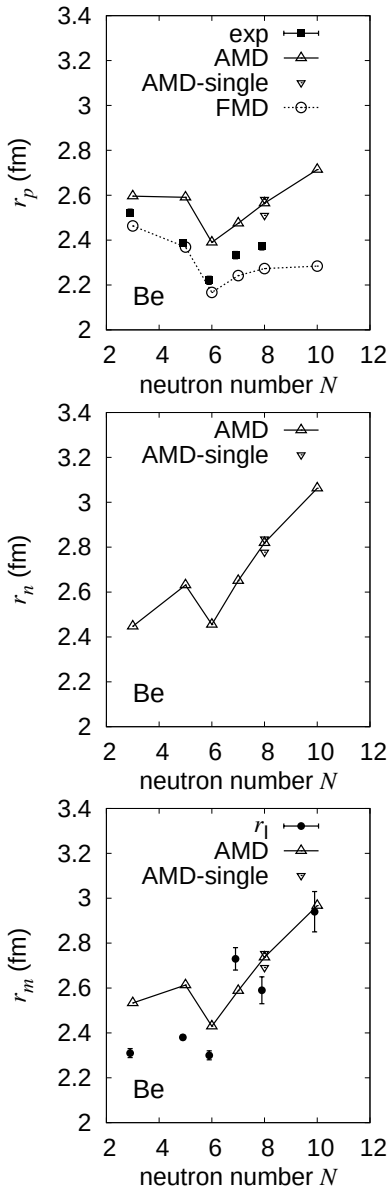


FIG. 2: Proton radii, neutron radii, and matter radii calculated with the AMD+VAP. For ^{12}Be, the radius calculated with the single AMD wave function for each of the 0_1^+ and 0_2^+ states before the superposition is also shown (AMD-single). The radii of AMD-single for the 0_1^+ are almost equal to those for the ground state after the superposition. The experimental proton radii are those reduced from the experimental charge radii [36, 37, 47]. The experimental matter radii ($r_{\rm I}$) deduced from the interaction cross section [49] are also shown.

[55].

In B isotopes, the charge radius is experimentally known only for ^{11}B. We show, in Fig. 3, the experimental data of proton radii $r_{\rm cc;G}$ deduced from the charge changing interaction cross section $\sigma_{\rm cc}$ by the Glauber analysis reported in Ref. [39]. We also show the proton radii $r_{\rm cc;S}$ evaluated from $\sigma_{\rm cc}$ in Ref. [48] using Eq. 6. The N dependence of $r_{\rm cc;S}$ is consistent with that of $r_{\rm cc;G}$ for ^{11}B, ^{13}B, and ^{15}B, but it is different at $N = 12$ for ^{17}B. The difference at $N = 12$, in principle, comes from the discrepancy of the $\sigma_{\rm cc}$ between two experiments in Ref. [48] and Ref. [39]. The present calculation with the AMD+VAP shows the N dependence consistent with $r_{\rm cc;G}$ deduced from $\sigma_{\rm cc}$ in Ref. [39].

The neutron and matter radii show the N dependence similar to each other. They show a kink at $N = 6$ and the increasing behavior in the $6 \leq N \leq 12$ region. The experimental matter radii $r_{\rm I}$ deduced from the interaction cross

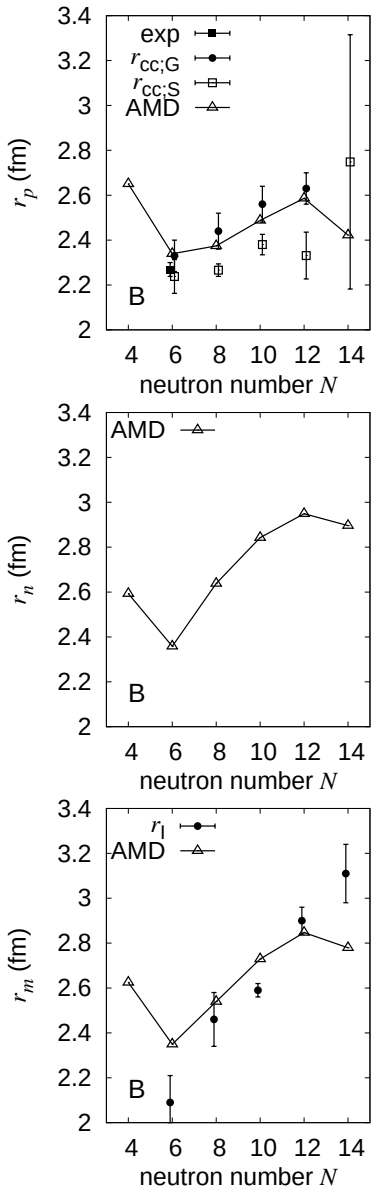


FIG. 3: Proton radii, neutron radii, and matter radii calculated with the AMD+VAP. The experimental proton radius for ^{11}B is reduced from the experimental charge radius [47]. The proton radii $r_{cc;G}$ deduced from the charge changing interaction cross section σ_{cc} by the Glauber analysis in Ref. [39], and the proton radii $r_{cc;S}$ evaluated from σ_{cc} in Ref. [48] using Eq. 6 are also shown. The experimental matter radii (r_I) are those deduced from the interaction cross section [49].

section show a monotonic increase of matter radii in the $6 \leq N \leq 14$ region and are consistent with the present result except for ^{19}B. The present calculation probably underestimates the large neutron radius of ^{19}B caused by a neutron halo structure.

The present calculation predicts the kink at $N = 6$ in the N dependences of proton, neutron, and matter radii, which is consistent with the experimental proton and matter radii. It is interesting that the kink exists not at the $N = 8$ magic number but at the $N = 6$ in B isotopes.

In order to discuss the N dependence of the proton radius around $N = 12$ in more details, we also investigate moments of the $J^\pi = 3/2^-$ ground states of B isotopes. Table I shows the calculated electric quadrupole moments (Q) and magnetic moments (μ) with the experimental data. It is found that the present calculation reasonably reproduces the Q moments of ^{11}B, ^{13}B, and ^{15}B, but it overestimates the Q moment of ^{17}B. Since the experimental

TABLE I: Electric quadrupole moments and magnetic dipole moments of B isotopes. Theoretical values are calculated with the AMD+VAP. The experimental data are taken from Refs. [50–54].

	AMD		exp.	
	$\mu(\mu_N)$	Q (mb)	$\mu(\mu_N)$	Q (mb)
^{9}B	2.65	6.54		
^{11}B	2.79	3.90	2.689	4.065(0.026)
^{13}B	2.97	3.65	3.178	3.693(0.11)
^{15}B	2.64	4.15	2.650(0.013)	3.80(0.10)
^{17}B	2.62	4.90	2.545(0.02)	3.86(0.15)
^{19}B	2.75	3.79		

μ moment is smallest in ^{17}B, it is likely that the contribution of the proton orbital angular momentum to the total spin $3/2^-$ is somewhat quenched in the realistic ground state of ^{17}B, which usually reduces the Q moment. Another possibility is the weakening of the cluster structure in ^{17}B, which reduces both the Q moment and r_p. In the present calculation, no quenching of proton orbital angular momentum contribution nor the weakening of cluster structure is obtained in ^{17}B. A more precise measurement of proton radii of ^{17}B is required.

D. C isotopes

The 0_1^+ and 2_1^+ states of C isotopes are calculated with the AMD+VAP. Figure 4 shows the binding energy, the 2_1^+ excitation energy, and $B(E2; 2_1^+ \to 0^+)$ of C isotopes. The present calculation reasonably reproduces the experimental data except for $E_x(2_1^+)$ in ^{20}C and the $B(E2)$ value in ^{14}C, which are overestimated by about a factor two.

Figure 5 shows the rms proton, neutron, and matter radii of C isotopes. Even though the neutron and matter radii increase in the $N \geq 6$ region as N increases, the proton radius is almost unchanged. The weak N dependence of the proton radius indicates the insensitivity of the proton distribution to the neutron structure. This is contrast to the cases of Be and B isotopes having the rather strong N dependence of proton radii. The N dependence of the matter radius in the present result is consistent with the experimental $r_{\rm I}$ deduced from the interaction cross section. The proton radii $r_{\rm cc;S}$ evaluated from the experimental data of the $\sigma_{\rm cc}$ at approximately 900 MeV/u show a weak N dependence in the $8 \leq N \leq 12$ region and seem to be consistent with the present prediction. There exists an experimental data of $r_{\rm cc;G}$ for ^{16}C deduced from the $\sigma_{\rm cc}$ at approximately 300 MeV by the Glauber analysis [38] seems to somewhat deviate from other data.

IV. DISCUSSIONS

In this section, we describe the intrinsic structure change with the increase of the neutron number in each series of isotopes and discuss its effect to the N dependence of proton radii.

Figure 6 shows the distributions of proton, neutron, and matter densities of Be, B, and C isotopes obtained by the AMD+VAP. The density distributions of intrinsic states before the spin and parity projections are displayed. In all series of Be, B, and C isotopes, the intrinsic neutron structures change rapidly with the increase of N.

In Be isotopes, the 2α cluster core structure is formed as shown in the dumbbell shape in the proton density. Following the development of the prolate neutron deformation, the cluster structure in Be isotopes is enhanced in the $7 \leq N \leq 10$ region, resulting in the increase of the proton radius in this region. Figure 7 shows the α-α distance measured by Gaussian centroids for four protons as $|\mathbf{X}_1 + \mathbf{X}_2 - \mathbf{X}_3 + \mathbf{X}_4|/2\sqrt{\nu}$, which indicates a degree of the 2α cluster development in Be isotopes. The α-α distance describes the N dependence of the proton radius in Be isotopes.

In B isotopes, the neutron density is most compact at $N = 6$ for ^{11}B because of the $p_{3/2}$ sub-shell closure feature. Also the proton structure in ^{11}B is compact and shows no cluster structure, whereas, in neutron-rich B isotopes with $N \geq 8$, the two-center cluster structure develops as shown in the proton distribution. The development of the cluster structure is remarkable at $N = 10$ and $N = 12$ for ^{15}B and ^{17}Be resulting in the enhanced proton radii of these nuclei, whereas it slightly weakens in ^{19}Be.

In C isotopes, the proton density always stays in a compact region in neutron-rich C with $N \geq 8$ even though the neutron structure rapidly changes with the increase of N. It indicates the robustness of the proton structure of $Z = 6$

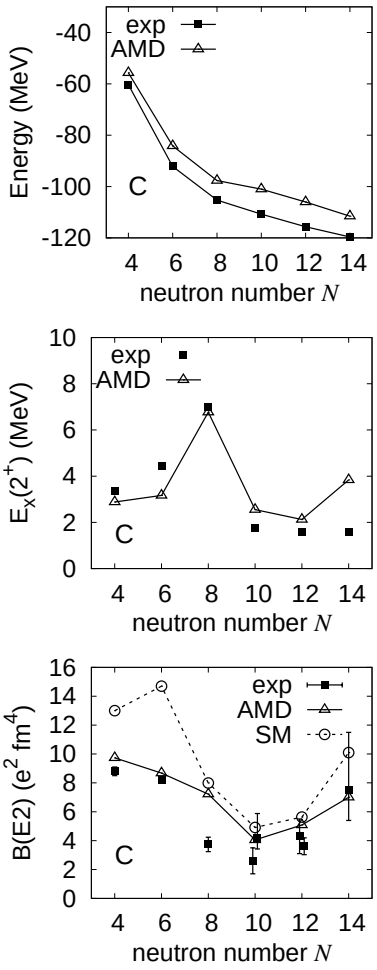


FIG. 4: Binding energy, 2^+ excitation energy, and $E2$ transition strength of C isotopes. The theoretical values are calculated with the AMD+VAP ($\nu = 0.19$ fm^{-2}) using MV1($m = 0.62$)+LS($u_I = -u_{II} = 2600$ MeV) force. The experimental data are taken from Refs. [50, 56–60]. Theoretical values for $B(E2)$ of the shell model calculation [61] are also shown.

system in neutron-rich C isotopes, in which protons are deeply bound. The stable proton structure is reflected in the weak N dependence of the proton radius.

As discussed above, in neutron-rich Be and B isotopes, which have two-center cluster structures, the proton structure changes sensitively to the neutron structure change. In contrast, in C isotopes, the proton structure is insensitive to the neutron structure and has the weak N dependence. The sensitivity of the proton structure to the neutron structure is essential in the N dependence of the proton radius. Development and weakening of the two-center cluster structures in Be and B isotopes play an important role in the change of proton radii with the N increase.

To see how the neutron structure change affects the N dependence of proton radii through the proton structure change, we show, in Fig. 8, the N dependence of the deformation parameters β_p and β_n for proton and neutron densities, respectively, in the intrinsic wave functions compared with the N dependence of proton radii in Be, B, and C isotopes. Here, the definition of β is that defined in Ref. [62].

In Be isotopes, the change of the proton deformation correlates with the neutron deformation except for ^{14}Be at $N = 10$. In ^{14}Be, the neutron deformation is not as large as that in ^{12}Be, but the wide distribution of the neutron density stretches the two-center proton density, resulting in the larger proton deformation than that in ^{12}Be. The proton deformation just describes the N dependence of the proton radius in Be isotopes.

Also in B isotopes, the change of proton deformation strongly correlates with the neutron deformation. The N dependence of the proton deformation is consistent with that of the proton radius in the neutron-rich $N \geq 8$ region, in which B isotopes have the two-center cluster structure as mentioned previously. However, in the region from $N = 6$

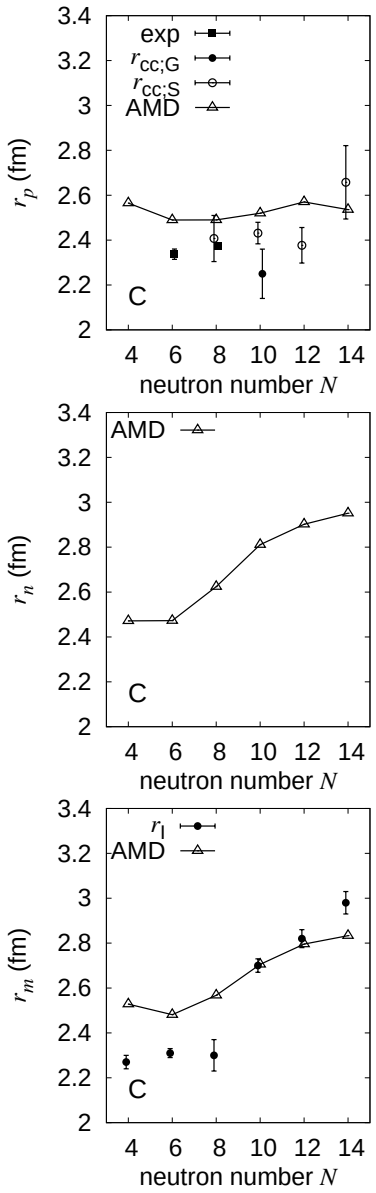


FIG. 5: Proton radii, neutron radii, and matter radii calculated with the AMD+VAP. The experimental proton radii for ^{12,14}C are reduced from the experimental charge radius [47]. The proton radius $r_{cc;G}$ of ^{16}C deduced from the σ_{cc} by the Glauber analysis in Ref. [38], and the proton radii $r_{cc;S}$ evaluated from the σ_{cc} in Ref. [48] using Eq. 6 are also shown. The experimental matter radii (r_I) are those deduced from the interaction cross section [49].

to $N = 8$, the N dependence of the proton radius is opposite to that of the proton deformation. Namely, the proton radius slightly increases from ^{11}B to ^{13}B even though the deformation becomes small at the neutron magic number $N = 8$. As discussed in the previous section, since ^{11}B has the smallest neutron radius and no cluster structure, it has the smallest proton radius in B isotopes.

In C isotopes, the change of β_p is consistent with β_n. Note that the consistency between β_p and β_n does not necessarily mean the consistency in the shapes between proton and neutron density distributions but the γ parameters for proton and neutron distributions are different from each other in some C isotopes. The N dependences of proton and neutron deformations in C isotopes are weaker than those in Be and B isotopes. Moreover, the change of proton deformation makes only the small change of the proton radii. This situation of neutron-rich C isotopes having no cluster structure is different from the cases of neutron-rich Be and B isotopes having two-center cluster structures, in

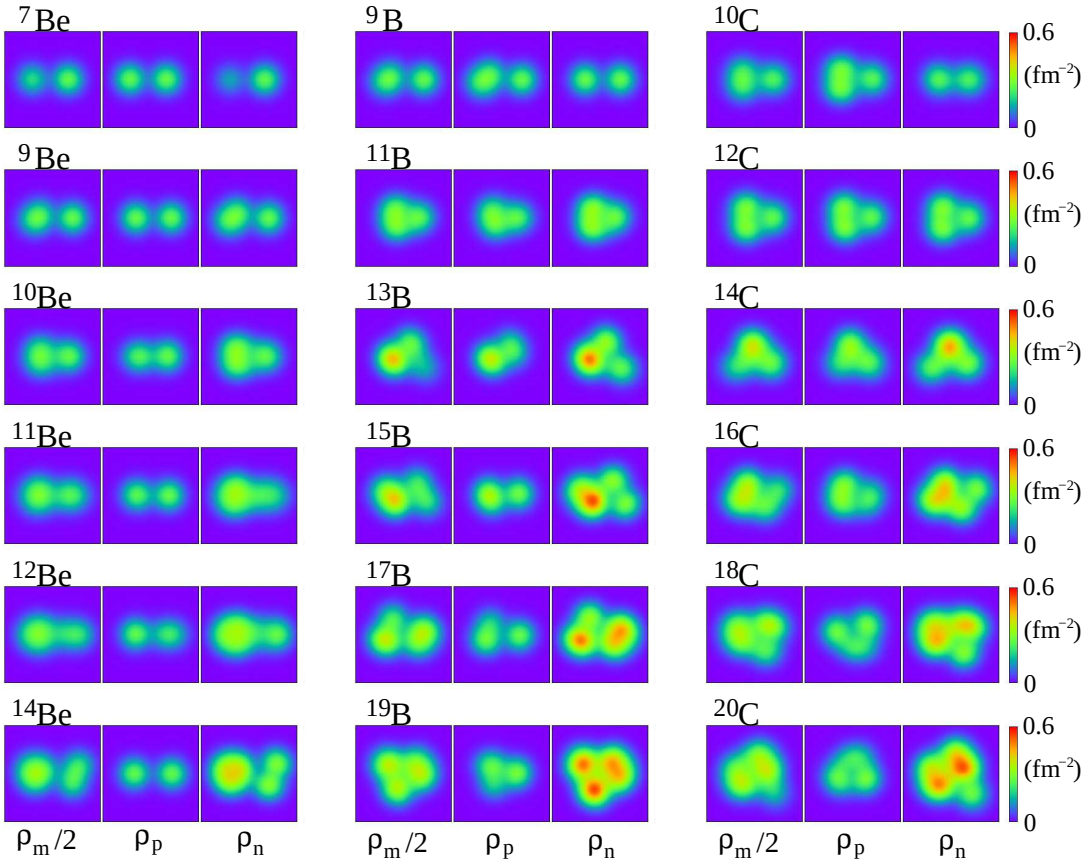


FIG. 6: (Color online) Distributions of proton, neutron, and matter densities calculated with the AMD+VAP. The densities of intrinsic states are integrated with respect to the z axis and plotted on x-y plane. Here, the axes of the intrinsic frame are chosen so as to be $\langle x^2\rangle \geq \langle y^2\rangle \geq \langle z^2\rangle$.

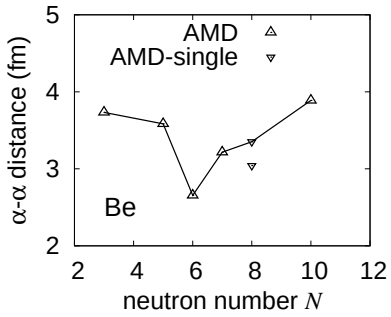


FIG. 7: α-α distance in Be isotopes.

which the proton radius correlates with the proton deformation. As a result, proton radii in C isotopes are insensitive to the neutron structure change and do not depend so much on the neutron number. The weak N dependence of the proton radius in C isotopes is considered to originate in stable oblate proton deformation and the non-cluster structure.

In the systematic analysis of the structure change and its effect on proton radii in Be, B, and C isotopes, we can reach the more general picture that, in light nuclei, the strong N dependence of proton radii is found in the isotopes

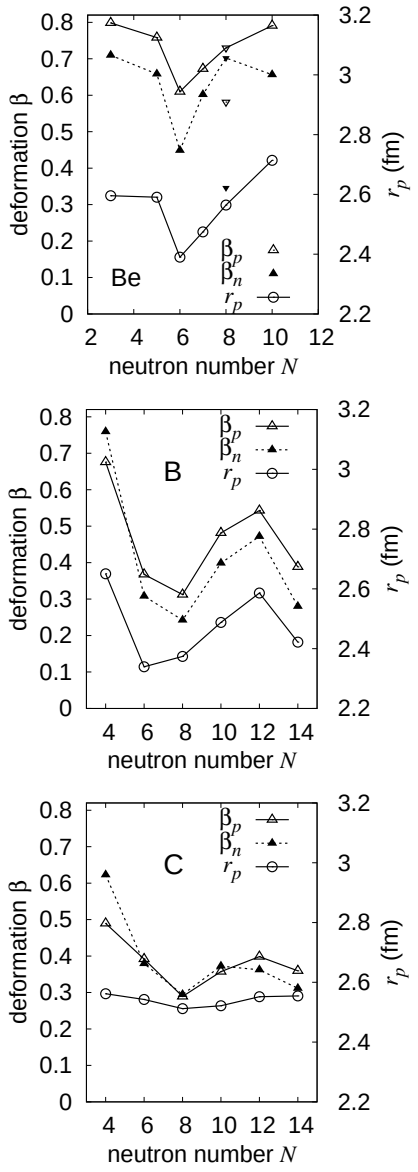


FIG. 8: Deformation parameter β for proton, neutron, and matter densities, and proton radii of Be, B, and C isotopes calculated with the AMD+VAP.

that have prolate deformations in both proton and neutron densities. In neutron-rich Be and B isotopes, the prolate proton deformation is caused by the development of two-center cluster structure. Since the cluster structure can be easily stretched by the prolate neutron deformation, the central proton density becomes low and the proton radii can be enhanced. In other words, the decrease of the central proton density in the developed cluster structure in neutron-rich nuclei is important in the sensitivity of proton radii to the structure change. Consequently, the N dependence of proton radii can be a probe to observe development of cluster structure. .

V. SUMMMARY

We investigated the N dependence of proton radii of Be, B, and C isotopes. In the result of the AMD+VAP calculation for Be and B isotopes, we found that the proton radius sensitively reflects the neutron structure change

through the the development of cluster structure, in particular, in neutron-rich nuclei. In contrast, the proton radius in C isotopes shows a weak N dependence because of the stability of the proton structure in $Z = 6$ nuclei. We compared the N dependence of the calculated proton radii with that of the experimental radii reduced from the charge radii measured by means of isotope shift and those deduced from the charge changing interaction cross section, and found that the present result is consistent with the existing experimental data.

In the analysis of the structure change and its effect on proton radii in Be, B, and C isotopes, we found that the N dependence of proton radii can be a probe to clarify enhancement and weakening of cluster structures. In neutron-rich Be and B nuclei, the two-center cluster structure is enhanced in the prolately deformed neutron structure. The N dependence of proton radii reflects rather sensitively the cluster structure change, because the central proton density becomes low in consequence of the stretching of the cluster structure. Precise measurements of proton radii for B and C isotopes are required to confirm the cluster structure in neutron-rich B isotopes and the non-cluster structure in C isotopes..

Acknowledgments

The author would like to thank Prof. Tanihata and Prof. Kanungo for fruitful discussions. She also thanks Prof. Kimura for valuable comments. The computational calculations of this work were performed using the supercomputer at YITP. This work was supported by JSPS KAKENHI Grant Number 26400270.

[1] W. von Oertzen, M. Freer and Y. Kanada-En'yo, Phys. Rep. **432**, 43 (2006).
[2] Y. Kanada-En'yo and H. Horiuchi, Prog. Theor. Phys. Suppl. **142**, 205 (2001).
[3] Y. Kanada-En'yo, M. Kimura and A. Ono, PTEP **2012** 01A202 (2012).
[4] M. Seya, M. Kohno, and S. Nagata, Prog. Theor. Phys. **65**, 204 (1981).
[5] W. von Oertzen, Z. Phys. A **354**, 37 (1996); **357**, 355 (1997),
[6] W. von Oertzen, Nuovo Cimento **110**, 895 (1997).
[7] Y. Kanada-En'yo, H. Horiuchi and A. Ono, Phys. Rev. C **52**, 628 (1995).
[8] K. Arai, Y. Ogawa, Y. Suzuki and K. Varga, Phys. Rev. C **54**, 132 (1996).
[9] A. Dote, H. Horiuchi and Y. Kanada-En'yo, Phys. Rev. C **56**, 1844 (1997).
[10] Y. Kanada-En'yo, H. Horiuchi and A. Doté, Phys. Rev. C **60**, 064304 (1999).
[11] N. Itagaki and S. Okabe, Phys. Rev. C **61**, 044306 (2000).
[12] N. Itagaki, S. Okabe and K. Ikeda, Phys. Rev. C **62**, 034301 (2000).
[13] Y.Ogawa, K.Arai, Y.Suzuki and K.Varga, Nucl. Phys. **A673**, 122 (2000).
[14] P. Descouvemont, Nucl. Phys. A **699**, 463 (2002).
[15] Y. Kanada-En'yo and H. Horiuchi, Phys. Rev. C **66**, 024305 (2002).
[16] Y. Kanada-En'yo and H. Horiuchi, Phys. Rev. C **68**, 014319 (2003).
[17] M. Ito, K. Kato and K. Ikeda, Phys. Lett. B **588**, 43 (2004).
[18] M. Ito, Phys. Lett. B **636**, 293 (2006).
[19] M. Freer, *et al.*, Phys. Rev. Lett. **82**, 1383 (1999); M. Freer, *et al.*, Phys. Rev. C **63**, 034301 (2001).
[20] A. Saito, *et al.*, Nucl. Phys. **A738**, 337 (2004); A. Saito, S. Shimoura, T. Minemura, Y. U. Matsuyama, H. Baba, N. Aoi, T. Gomi and Y. Higurashi *et al.*, Mod. Phys. Lett. A **25**, 1858 (2010).
[21] N. Curtis *et al.*, Phys. Rev. C **70**, 014305 (2004).
[22] M. Milin *et al.*, Nucl. Phys. **A753**, 263 (2005).
[23] M. Freer *et al.*, Phys. Rev. Lett. **96**, 042501 (2006).
[24] H. G. Bohlen, T. Dorsch, T. Kokalova, W. von Oertzen, C. Schulz and C. Wheldon, Phys. Rev. C **75**, 054604 (2007).
[25] N. Curtis, N. I. Ashwood, M. Freer, T. Munoz-Britton, C. Wheldon, V. A. Ziman, S. Brown and W. N. Catford *et al.*, J. Phys. G **36**, 015108 (2009).
[26] Z. H. Yang, *et al.*, Phys. Rev. Lett. **112**, 162501 (2014).
[27] T. Suzuki and T. Otsuka, Phys. Rev. C **56**, 847 (1997).
[28] A. Navin *et al.*, Phys. Rev. Lett. **85**, 266 (2000).
[29] S. D. Pain *et al.*, Phys. Rev. Lett. **96**, 032502 (2006).
[30] H. Iwasaki *et al.*, Phys. Lett. B **481**, 7 (2000).
[31] H. Iwasaki *et al.*, Phys. Lett. B **491**, 8 (2000).
[32] S. Shimoura *et al.*, Phys. Lett. B **560**, 31 (2003).
[33] Y. Kanada-En'yo and H. Horiuchi, Phys. Rev. C **52**, 647 (1995).
[34] G. Thiamova, N. Itagaki, T. Otsuka, and K. Ikeda, Eur. Phys. J. A **22**, 461 (2004).
[35] Y. Kanada-En'yo, Phys. Rev. C **71**, 014310 (2005).

[36] W. Nortershauser, D. Tiedemann, M. Zakova, Z. Andjelkovic, K. Blaum, M. L. Bissell, R. Cazan and G. W. F. Drake *et al.*, Phys. Rev. Lett. **102**, 062503 (2009).

[37] A. Krieger, K. Blaum, M. L. Bissell, N. Frommgen, C. Geppert, M. Hammen, K. Kreim and M. Kowalska *et al.*, Phys. Rev. Lett. **108**, 142501 (2012).

[38] T. Yamaguchi, I. Hachiuma, A. Kitagawa, K. Namihira, S. Sato, T. Suzuki, I. Tanihata and M. Fukuda, Phys. Rev. Lett. **107**, 032502 (2011).

[39] A. Estradé, *et al.*, Phys. Rev. Lett. **113**, 132501 (2014).

[40] H. Feldmeier, K. Bieler and J. Schnack, Nucl. Phys. A **586**, 493 (1995).

[41] T. Neff and H. Feldmeier, Nucl. Phys. A **713**, 311 (2003).

[42] N. Furutachi, M. Kimura, A. Doté, and Y. Kanada-En'yo, Prog. Theo. Phys. **122**, 865 (2009).

[43] T. Ando, K. Ikeda and A. Tohsaki, *Prog. Theory. Phys.* **64**, 1608 (1980).

[44] N. Yamaguchi, T. Kasahara, S. Nagata and Y. Akaishi, *Prog. Theor. Phys.* **62**, 1018 (1979); R. Tamagaki, *Prog. Theor. Phys.* **39**, 91 (1968).

[45] Y. Kanada-En'yo, Phys. Rev. Lett. **81**, 5291 (1998).

[46] Y. Kanada-En'yo, Prog. Theor. Phys. **117**, 655 (2007) [Erratum-ibid. **121**, 895 (2009)].

[47] I. Angeli, At. Data Nucl. Data Tables **87**, 185 (2004).

[48] L. V. Chulkov *et al.*, Nucl. Phys. A **674** 330 (2000).

[49] A. Ozawa, T. Suzuki and I. Tanihata, Nucl. Phys. A **693**, 32 (2001).

[50] D. R. Tilley *et al.*, Nucl. Phys. A **745**, 155 (2004).

[51] H. Okuno, *et al.*, Phys. Lett. B **354**, 41 (1995).

[52] H. Ueno, K. Asahi, H. Izumi, K. Nagata, H. Ogawa, A. Yoshimi, H. Sato and M. Adachi *et al.*, Phys. Rev. C **53**, 2142 (1996).

[53] H. Izumi, K. Asahi, H. Ueno, H. Okuno, H. Sato, K. Nagata, Y. Hori and M. Adachi *et al.*, Phys. Lett. B **366**, 51 (1996).

[54] H. Ogawa, K. Asahi, K. Sakai, T. Suzuki, H. Izumi, H. Miyoshi, M. Nagakura and K. Yogo *et al.*, Phys. Rev. C **67**, 064308 (2003).

[55] Y. Kanada-En'yo, Phys. Rev. C **71**, 014303 (2005).

[56] E. A . McCutchan, C. J. Lister, S. C. Pieper, R. B. Wiringa, D. Seweryniak, J. P. Greene, P. F. Bertone and M. P. Carpenter *et al.*, Phys. Rev. C **86**, 014312 (2012).

[57] M. Wiedeking, P. Fallon, A. O. Macchiavelli, J. Gibelin, M. S. Basunia, R. M. Clark, M. Cromaz and M. -A. Deleplanque *et al.*, Phys. Rev. Lett. **100**, 152501 (2008).

[58] H. J. Ong, N. Imai, D. Suzuki, H. Iwasaki, H. Sakurai, T. K. Onishi, M. K. Suzuki and S. Ota *et al.*, Phys. Rev. C **78**, 014308 (2008).

[59] P. Voss, T. Baugher, D. Bazin, R. M. Clark, H. L. Crawford, A. Dewald, P. Fallon and A. Gade *et al.*, Phys. Rev. C **86**, 011303 (2012).

[60] M. Petri, P. Fallon, A. O. Macchiavelli, S. Paschalis, K. Starosta, T. Baugher, D. Bazin and L. Cartegni *et al.*, Phys. Rev. Lett. **107**, 102501 (2011).

[61] H. Sagawa, X. R. Zhou, X. Z. Zhang and T. Suzuki, Phys. Rev. C **70**, 054316 (2004).

[62] Y. Kanada-En'yo and H. Horiuchi, Phys. Rev. C **55**, 2860 (1997).